Hurricane "Rainfall Potential" Derived from Satellite Observations Aids Overland Rainfall Prediction

HAIYAN JIANG*

Joint Center for Earth Systems Technology, University of Maryland, Baltimore County, Baltimore, and Mesoscale Atmospheric Processes Branch, NASA Goddard Space Flight Center, Greenbelt, Maryland

JEFFREY B. HALVERSON

Joint Center for Earth Systems Technology, University of Maryland, Baltimore County, Baltimore, Maryland

JOANNE SIMPSON

Laboratory for Atmospheres, NASA Goddard Space Flight Center, Greenbelt, Maryland

EDWARD J. ZIPSER

Department of Meteorology, University of Utah, Salt Lake City, Utah

(Manuscript received 18 October 2006, in final form 29 June 2007)

ABSTRACT

The Tropical Rainfall Measuring Mission–based National Aeronautics and Space Administration Goddard Multisatellite Precipitation Analysis (MPA) product is used to quantify the rainfall distribution in tropical cyclones that made landfall in the United States during 1998–2004. A total of 37 tropical cyclones (TC) are examined, including 2680 three-hourly MPA precipitation observations. Rainfall distributions for overland and overocean observations are compared. It is found that the TC rainfall over ocean bears a strong relationship with the TC maximum wind, whereas the relationship for overland conditions is much weaker. The rainfall potential is defined by using the satellite-derived rain rate, the satellite-derived storm size, and the storm translation speed. This study examines the capability of the overocean rainfall potential to predict a storm's likelihood of producing heavy rain over land. High correlations between rain potentials before landfall and the maximum storm total rain over land are found using the dataset of the 37 landfalling TCs. Correlations are higher with the average rain potential on the day prior to landfall than with averages over any other time period. A TC overland rainfall index is introduced based on the rainfall potential study. This index can be used to predict the storm peak rainfall accumulation over land. Six landfalling storms during the 2005 Atlantic Ocean hurricane season are examined to verify the capability of using this index to forecast the maximum storm total rain over land in the United States. The range of the maximum storm overland rain forecast error for these six storms is between 2.5% and 24.8%.

1. Introduction

Predicting hurricane landfall precipitation is a major operational challenge. Inland flooding has become the predominant cause of deaths associated with hurricanes in the United States (Rappaport 2000). Skill in tropical cyclone (TC) track forecasting has improved by 20% over the last five years, achieving the first goal set by the U.S. Weather Research Program Hurricane Landfall program (HL). The HL (Elsberry 2005) focuses on improving predictions of TC track, intensity change, and precipitation. However, the difficulties of improving 72-h quantitative precipitation forecasts for TCs, thereby improving day-3 forecasts for inland flooding, have long been recognized (Elsberry 2002). The distribution of TC instantaneous and accumulated rainfall is multiscale in nature. Mesoscale convective systems modulate a significant amount of TC rain, but their space and time variations are not well understood

* Current affiliation: Department of Meteorology, University of Utah, Salt Lake City, Utah.

Corresponding author address: Dr. Haiyan Jiang, 135 S 1460 E, Rm. 819 WBB, Salt Lake City, UT 84112.
E-mail: h.jiang@utah.edu

DOI: 10.1175/2007JAMC1619.1

(Heymsfield et al. 2001). Once a storm makes landfall, additional factors such as the presence of significant topography and extratropical transition of the cyclone involving jet streak, trough, and frontal interactions come into play (Carr and Bosart 1978; Atallah and Bosart 2003). It has been noted that some of the most devastating floods are produced by tropical systems in the weak end of the spectrum—for example, Tropical Storm Allison [2001; $6 billion in damages, 27 deaths, and 35–40 in. of rain (1 in. $\simeq$ 2.54 cm)] and Tropical Storm Claudette (1979; 42 in. of rain in 24 h).

Early precipitation studies of TCs over land have been confined to rain gauge and radar data. Miller (1958) examined the composite and frequency distribution of hourly rain amounts for 16 Florida hurricanes with respect to their center. He found that the mean rain rate in the 1° box directly surrounding the storm center was about a factor of 2 higher than the mean rain rate in the remaining outer domain. Significant asymmetric characteristics of the hurricane rainfall over land were also recognized (Atallah and Bosart 2003).

Satellites provide the most common means for monitoring TC rainfall over ocean. Satellite-based statistical analysis of TC rainfall characteristics is critical to understanding and improving quantitative precipitation forecasts in TCs. With different satellite observations and sample sizes, various studies have looked at radial distributions of TC instantaneous rainfall. The observations they used vary from the *Nimbus-5* Electrically Scanning Microwave Radiometer (ESMR-5; Rodgers and Adler 1981) to the Special Sensor Microwave Imager (SSM/I; Rao and MacArthur 1994; Rodgers and Pierce 1995; Rodgers et al. 1994), to the Tropical Rainfall Measuring Mission (TRMM) Microwave Imager (TMI; Lonfat et al. 2004). The sample size varies from less than 100 satellite observations for several TCs in one or two basins to over 2000 TMI observations for 260 TCs over the global oceans (Lonfat et al. 2004). Most of these studies analyzed overocean samples. Only one study (Rao and MacArthur 1994) analyzed the land–ocean combined sample, but most observations were over the ocean. Major findings of these studies are that the instantaneous rainfall increases with storm intensity and that the inner-core (within 100 km of the storm center) mean rain rate of major hurricanes is about 2–3 times that of tropical storms.

The first goal of this study is to determine the differences of TC rainfall distributions for conditions over ocean versus conditions over land. This analysis uses a 3-hourly instantaneous rainfall product, which is the National Aeronautics and Space Administration (NASA) Multisatellite Precipitation Analysis (MPA) product (TRMM 3B42).

When the storm is over ocean, its rain is correlated well with storm maximum wind intensity; over land, this kind of relationship might be much weaker because of additional factors. Hurricanes or typhoons, and even tropical storms, can produce torrential rains during landfall. Floods by TCs are associated not only with the storm's maximum wind intensity but also with its history, its projected movement, and its size. Regardless of the complicated factors such as topography and trough interactions that influence the hurricane landfall and inland rainfall, Malkus and Riehl (1960) found that the cloud–rain pattern of many storms was very similar from day to day. In addition, Griffith et al. (1978) noted great variability in storm total accumulated rainfall from system to system. Griffith et al. (1978) further proposed a hypothesis that known information about the rainfall history or "wetness" of a storm as it evolves over ocean may be used to predict the storm's potential for catastrophic inland flooding. They defined a parameter called rainfall potential, which is defined by using an estimated average rain rate derived from infrared (IR) satellite observations, combined with the storm size and translation speed information. The rainfall potential histories of a dozen TCs approaching landfall were examined. Their method correctly predicted the highest actual rainfall totals for the major flood hurricanes Agnes (1972) and Fifi (1974) and the lowest potentials for the relatively dry hurricanes Celia (1970) and Edith (1971). A similar technique called the tropical rainfall potential (TRaP) was developed at the National Oceanic and Atmospheric Administration/National Environmental Satellite, Data, and Information Service (NOAA/NESDIS; Kidder et al. 2005; Ferraro et al. 2005). TRaP uses the SSM/I, the Advanced Microwave Sounding Unit (AMSU), and the TMI rain rates to predict tropical cyclone rainfall potential. Ferraro et al. (2005) found that the TMI TRaPs performed better than the AMSU TRaPs and SSM/I TRaPs.

With the advantages of better physical connection between microwave observations and precipitation and high spatial and temporal resolution of IR observations, a combined microwave–IR rainfall product can provide better precipitation estimates globally than any microwave- or IR-only products (Adler et al. 1993, 1994, 2003; Huffman et al. 2001). In the framework of the TRMM project, MPA has produced gridded 3-hourly precipitation rate estimates with relatively high horizontal resolution (0.25° $\times$ 0.25° longitude/latitude) since January of 1998. These rainfall estimates are based on microwave information provided by various low-orbiting satellites, merged with IR-based estimates from geostationary meteorological satellites (Huffman et al. 2007). TRMM products are used to

calibrate the estimates. Applying the new real-time MPA rainfall estimates to Griffith et al.'s (1978) technique, Jiang et al. (2008a,b) examined the difference in rainfall potential history and water budget of Hurricanes Isidore and Lili (both 2002). Isidore produced much heavier rain as a greatly weakened tropical storm than did category-1 Hurricane Lili during landfall over the same area. Jiang et al. (2008a) showed that the average rainfall potential during 4 days before landfall for Isidore was a factor of more than 2.5 higher than that for Lili. Jiang et al. (2008b) explained that the difference in the landfall rain amounts of these two storms is partially due to the larger diameter of Isidore. More important, however, the water vapor budget study in Jiang et al. (2008b) demonstrated that Isidore was initially a wet storm (with higher storm total accumulated rainfall) and that its volumetric total precipitable water was larger and extended to a larger radius than Lili's during their whole lifetime. The second goal of this study is to examine the relationships between the rain potential before landfall and maximum storm total rainfall over land for the landfalling TCs over the North Atlantic Ocean during 1998–2004 by using the 3-hourly MPA product.

Section 2 presents a description of MPA data, the definition of rain potential, the method used to analyze the MPA rainfall parameters and case studies, and hurricane best-track and overland rain information. Section 3 uses the MPA rainfall product to determine the rainfall distribution of North Atlantic TCs during 1998–2004 over ocean and land. Section 4 presents the relationships between rain potentials before landfall and maximum storm total rainfall over land, and it introduces an index for TC overland rain forecasting. Section 5 includes a summary, a discussion, and a description of future work. The limitations of the prediction index are discussed in both sections 4 and 5.

2. Data and methods

a. MPA product

The NASA Goddard MPA product used in this study is based on two different sets of sensors. Microwave data are collected by various low-orbit satellites, including the TMI, the SSM/I, the Advanced Microwave Scanning Radiometer for the Earth Observing System (AMSR-E), and the AMSU. Precipitation estimates are derived from TMI, SSM/I, and AMSR-E microwave data by applying the Goddard profiling algorithm (GPROF; Kummerow et al. 1996). AMSU microwave measurements are converted to rainfall estimates by using the AMSU-B algorithm (Zhao and Weng 2002; Weng et al. 2003). High-quality (HQ) microwave estimates are produced by using the TRMM combined instrument (TCI) to calibrate microwave precipitation estimates. The TCI utilizes the superior horizontal resolution of the TMI and TRMM precipitation radar to produce an HQ merged microwave rainfall estimate. The IR data are collected by the international constellation of geosynchronous Earth orbit (GEO) satellites. The IR estimates are calibrated with the HQ microwave estimates. The microwave and GEO–IR estimates are merged in a probability-matching method (Huffman et al. 2007). A post-real-time product called MPA (in the framework of TRMM, it is also called TRMM 3B42) is produced from the merged microwave–IR dataset. The MPA dataset consists of gridded 3-hourly precipitation rate files with $0.25° \times 0.25°$ longitude/latitude horizontal resolution within the global latitude belt from 50°S to 50°N. The temporal resolution is 3 h, and the files are generated on synoptic observations times (0000 UTC, 0300 UTC, . . . , 2100 UTC). In this study, the TRMM version 6 of the MPA product is used.

b. Tropical cyclone best-track and overland rain information

North Atlantic TC postanalysis best tracks for 1998–2004 were provided by the National Hurricane Center (NHC, now known as the Tropical Prediction Center). The extended best-track dataset for 1988–2004 was created by M. DeMaria at Colorado State University to include storm size information that was not in the standard NHC best-track data (Demuth et al. 2006). The postanalysis merges available data to produce a (sometimes smoothed) time history of the cyclone's center position, maximum sustained winds, and minimum sea level pressure for every 6 h. The available data sources include ship and other surface reports, aircraft reconnaissance data, and satellite imagery. At present, there are no error estimates for these variables. These parameters are generally more reliable west of 55° longitude, where aircraft reconnaissance data are usually available.

According to the best-track information, a dataset including 37 North Atlantic TCs that made landfall in the United States during 1998–2004 is constructed. For each landfalling TC, its maximum storm total rain accumulation over land was provided by the tropical cyclone rainfall data Internet page (http://www.hpc.ncep.noaa.gov/tropical/rain/tcrainfall.html) built by D. Roth at the NOAA Hydrometeorological Prediction Center. This TC overland rainfall database is based on rain gauge observations from the National Climatic

TABLE 1. Parameters of the 37 North Atlantic landfalling TCs during 1998–2004 derived from the NHC best-track data and rain gauge observations (see text for details). An asterisk following the storm name represents storms with multiple landfalls in the United States. A pound sign represents storms that experienced a translation speed change of more than a factor of 2 during 24 h before and after landfall time. Also, note that Hurricane Gustav (2002) did not have any U.S. landfall, but its center was very close to the East Coast on 10 Sep 2002. The landfall time indicated here is the approximate time at which its track was the closest to the coast.

Year	Name	Max wind during the whole lifetime (kt; 1 kt ≈ 0.5 m s^{-1})	U.S. landfall time	Max wind at the U.S. landfall time (kt)	Land-rain period in the United States	Storm translation speed at landfall day (km day^{-1})	Storm size parameter $\bar{d}$ at landfall day (km)	Max storm total rain during landfall in the United States (mm)
1998	Bonnie	100	0400 27 Aug	95	26–29 Aug	284	889	371.09
1998	Charley	60	1000 22 Aug	40	20–25 Aug	271	944	483.87
1998	Earl	85	0600 3 Sep	70	1–6 Sep	803	1222	415.54
1998	Frances	55	0600 11 Sep	45	7–17 Sep	310	1667	568.71
1998	Georges*	135	1530 25 Sep	90	24 Sep–1 Oct	399	1000	976.88
1998	Hermine	40	0500 20 Sep	35	17–22 Sep	445	889	359.16
1998	Mitch	155	1100 5 Nov	55	4–5 Nov	1564	2222	284.48
1999	Bret	125	0000 23 Aug	100	22–25 Aug	232	556	334.77
1999	Dennis	90	2100 4 Sep	60	24 Aug–6 Sep	365	1833	350.52
1999	Floyd	135	0630 16 Sep	90	14–17 Sep	1078	2222	611.12
1999	Harvey#	50	1700 21 Sep	50	19–22 Sep	1237	1667	254.00
1999	Irene*	95	1300 15 Oct	65	12–17 Oct	428	1333	443.23
2000	Gordon	70	0300 18 Sep	55	14–21 Sep	624	1222	240.79
2000	Helene	60	1200 22 Sep	35	19–24 Sep	767	1333	243.84
2001	Allison*	50	2100 5 Jun	45	4–17 Jun	344	889	1033.27
2001	Barry	60	0500 6 Aug	60	1–8 Aug	473	778	297.18
2001	Gabrielle	70	1200 14 Sep	60	10–16 Sep	338	1111	383.54
2002	Bertha*	35	0800 9 Aug	20	3–9 Aug	272	167	260.35
2002	Edouard	55	0045 5 Sep	35	2–7 Sep	311	778	194.06
2002	Fay#	50	0900 7 Sep	50	5–11 Sep	371	1555	469.65
2002	Gustav	85	1800 10 Sep	55	8–12 Sep	810	1222	152.40
2002	Hanna*	50	1500 14 Sep	50	12–15 Sep	499	1555	395.22
2002	Isidore	110	0600 26 Sep	55	20–29 Sep	718	1944	469.90
2002	Kyle	75	2200 11 Oct	35	9–12 Oct	900	1389	221.49
2002	Lili	125	1300 3 Oct	80	2–5 Oct	808	1055	213.36
2003	Bill	50	1900 30 Jun	50	27 Jun–3 Jul	636	1222	259.08
2003	Claudette	75	1530 15 Jul	80	14–18 Jul	545	722	168.15
2003	Grace	35	1100 31 Aug	35	30 Aug–4 Sep	407	1444	263.14
2003	Henri#	50	0900 6 Sep	30	2–17 Sep	505	1167	230.89
2003	Isabel	145	1700 18 Sep	90	17–21 Sep	1028	1555	513.08
2004	Bonnie#	55	1400 12 Aug	40	11–14 Aug	1186	1889	154.18
2004	Charley*	125	2045 13 Aug	125	12–15 Aug	1290	1555	250.95
2004	Frances*	125	1800 6 Sep	50	3–11 Sep	327	778	598.68
2004	Gaston	65	1400 29 Aug	65	25 Aug–1 Sep	328	833	320.04
2004	Ivan*	145	0650 16 Sep	105	13–26 Sep	565	1500	431.80
2004	Jeanne	105	0400 26 Sep	105	25–30 Sep	448	889	304.04
2004	Matthew	40	1100 10 Oct	35	6–15 Oct	648	2222	457.20

Data Center, National Weather Service River Forecast Centers, many local water management networks, and additional NHC reports (D. Roth 2005, personal communication). The maximum storm total rain represents the maximum value of the storm-accumulated rains during the storm's U.S. land-rain period (the days on which the storm rains over the U.S. land) for all rain gauge stations. Table 1 lists the 37 landfalling TCs, their maximum surface wind during their whole lifetime, U.S. landfall time (when the storm center is over land),[1] maximum surface wind at the U.S. landfall time, U.S. overland rain period, maximum storm total rains during U.S. overland period, translation speed at the day of landfall (the period of 24 h after the U.S.

[1] Some storms had multiple landfalls in the United States. In this database, we include only one landfall time for each storm, with the landfall location closest to the station of the maximum storm total rain over land.

landfall time), and MPA estimated storm size parameter $\overline{d}$ (daily mean cross section; see section 2c for a detailed definition of $\overline{d}$) at the day of landfall. The samples in Table 1 include all of the time periods during which storms were reported in the NHC best track, including extratropical and subtropical stages.

c. Definition of rain potential

This study applies the hypothesis proposed by Griffith et al. (1978) to assess the flooding potential of approaching TCs using a parameter called mean total rain potential, defined as

$$\text{mean total rain potential} = \overline{D}\,\overline{d}/\overline{v}, \tag{1}$$

where $\overline{D}$ is MPA daily average storm rainfall (mm day^{-1}). We draw a circle around the rain area on the MPA daily rainfall accumulation image by excluding rain that is not associated with the tropical cyclone. Here, $\overline{D}$ is averaged inside the circle, and $\overline{d}$ is the mean cross section (km) of the storm as measured from the satellite image in the direction of motion according to Griffith et al.'s (1978) definition. In this study, $\overline{d}$ is determined subjectively from the MPA daily rain accumulation image, where a line is drawn and measured for continuous rain area in the direction of storm motion. The $\overline{v}$ is the mean storm translation speed (km day^{-1}) derived from hurricane best-track data. It is realized that the expected duration of rainfall at a point as a tropical cyclone passes overhead is approximately $\overline{d}/\overline{v}$. The mean total rainfall, then, would be $(\overline{D}\,\overline{d})/\overline{v}$. This definition is the same as the TRaP used in Kidder et al. (2000, 2005). Equation (1) has a problem if the storm is stationary; however, there is not that kind of extreme case in the storm samples used in this study. Kidder et al. (2005) used an areal TRaP technique that seems to be able to eliminate this problem. In their technique, as the speed of the storm approaches zero, the mean rain potential is simply the mean daily rain.

d. Analysis method

To determine the rainfall characteristics of TC over ocean and land, a total of 2680 three-hourly MPA observations for the whole lifetime of the 37 TCs are grouped into overocean and overland categories. The criterion is if one observation contains 60% of rain pixels over ocean (land), then this observation is attributed to the overocean (overland) category. Observations that are not identified as either overland or overocean are called mixed. The data are also categorized by the storm intensity stage: tropical depressions (TD) are defined as systems with maximum wind speed of less than 17 m s^{-1}, tropical storms (TS) are systems with maximum wind speed between 18 and 33 m s^{-1}, and hurricanes (HURs) are systems with maximum wind speed that is greater than 34 m s^{-1}. Table 2 shows the number of MPA observations for each category. The MPA rainfall parameters are derived in storm-relative coordinates. The storm motion and intensity change are neglected during the MPA 3-h window. This could cause some errors in analyzing the radial distribution of TC rainfall for different intensity categories. The azimuthal averages are calculated in 28-km-wide annuli (according to the 0.25°-resolution of MPA data) around the storm center outward to the 1111-km radius for MPA-derived parameters. We choose this 10° radius to capture extreme storm sizes. The resulting dataset allows us to examine the radial dependence of parameters as a function of time. The conditional (only when raining) probability density functions (PDF) of rain rate with radial distance can also be determined using the annular dataset. Using the annular PDFs, a contoured diagram of frequency by radial distance (2D frequency) can be constructed as a function of storm intensity and location (e.g., over ocean or land).

TABLE 2. The number of MPA observations for each category.

	TD	TS	HUR	Total
Over ocean	482	790	713	1985
Over land	284	117	20	421
Mixed	116	105	53	274
Total	882	1012	786	2680

3. Distribution of TC rainfall over land and ocean

In this section, the distribution of TC rainfall derived from the MPA product is presented. The comparison with previous studies on the distribution of TC rainfall is also presented. The numerical study by Rogers et al. (2003) shows that the asymmetry could be significantly different between instantaneous and accumulated TC rainfall depending on the relative orientation of the shear and storm motion vectors. However, because we are mainly comparing the distribution of azimuthally averaged rain, no asymmetric information could be resolved.

a. PDF of rain rates

Figure 1 shows the PDF distributions of rain rates for all MPA rainfall observations within an area of 1111 km (10° radius) around the storm center. The mode is near 1 mm h^{-1} but is not the same for different subsamples: the overocean PDF has a mode of 1 mm h^{-1} and the

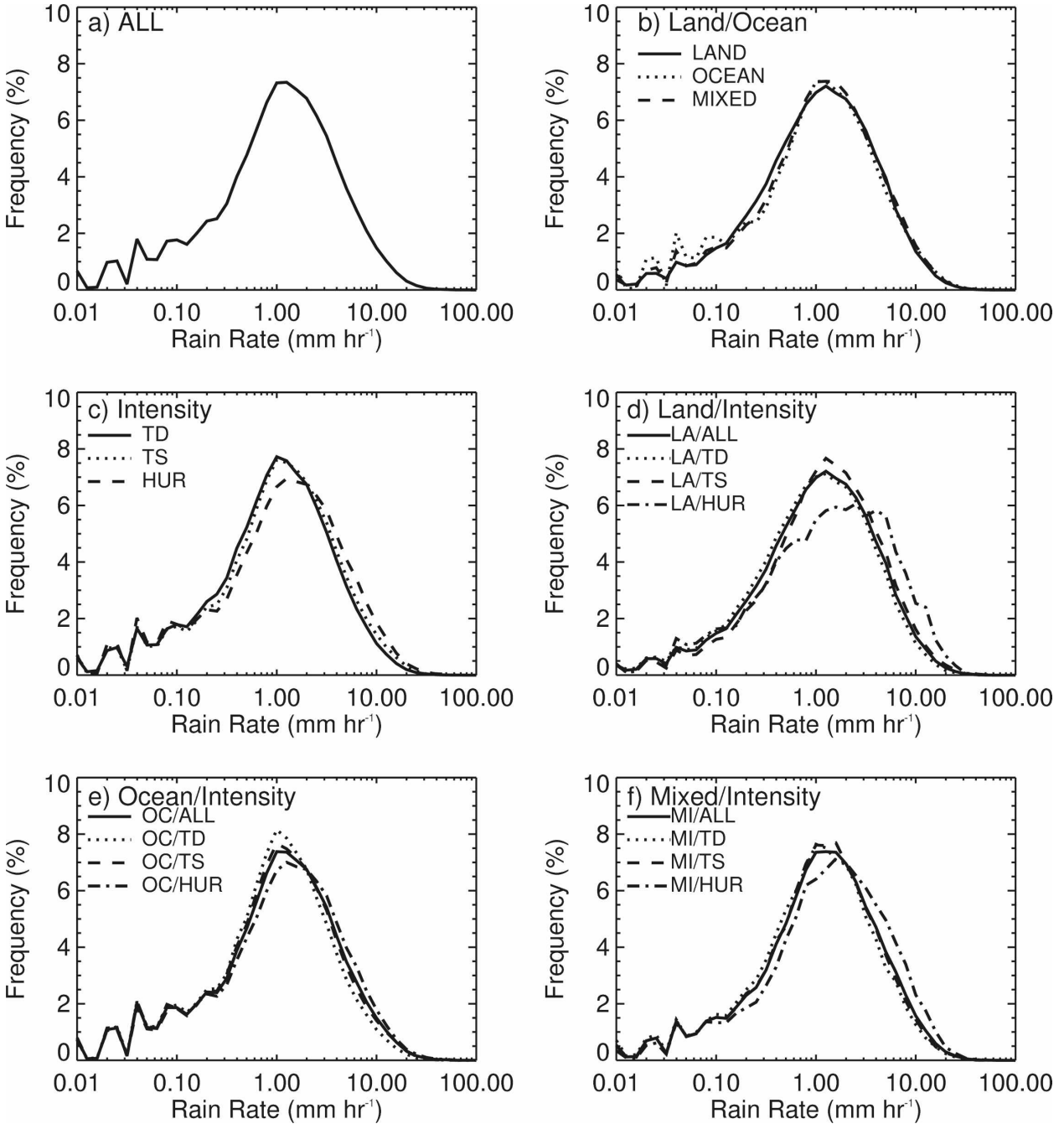

FIG. 1. Probability density functions calculated within 10° radius of storm center for (a) all 2680 observations, (b) overland and overocean groups, (c) TC intensity groups, (d) overland intensity subgroups, (e) overocean intensity subgroups, and (f) mixed intensity subgroups.

overland and mixed PDFs show a mode of about 1.2 mm h^{-1} (Fig. 1b). Not only are the modes of overland and mixed distributions higher than that for the overocean distribution but also the overland and mixed distributions tend to be broader than the overocean distribution. For the TC intensity groups (Fig. 1c), as the storm intensity increases, the mode of the distribution shifts toward higher values and the distribution tends to become broader. This is similar to what is documented by Lonfat et al. (2004), although our analysis bears an error caused by the storm motion during the 3-h MPA data window.

Similar characteristics can be seen in the different intensity PDFs for overland (Fig. 1d), overocean

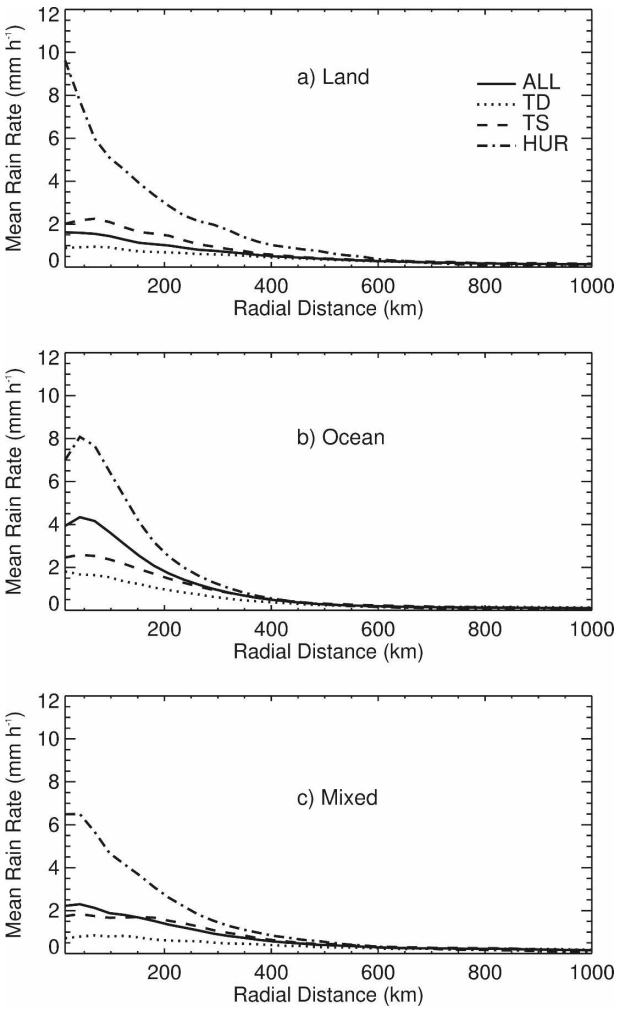

FIG. 2. Mean rain rates as a function of radial distance for different TC intensity for (a) overland, (b) overocean, and (c) mixed categories.

(Fig. 1e), and mixed (Fig. 1f) groups. The land TD distribution is similar to the overall overland PDF, which is not surprising because a greater percentage of overland observations are in depression stage as a result of the land interaction effect decreasing the storm intensity. Both land TS and land HUR PDFs have higher modes and broader distributions than those of overall TS and HUR PDFs (Fig. 1c), which indicates that HUR and TS peak rains tend to be stronger over land than over ocean. All of the overocean TD, TS, and HUR distributions (Fig. 1e) are similar to the overall TD, TS, and HUR PDFs (Fig. 1c) because of the greater number of overocean observations. In summary, for all storm intensities, overocean PDFs are narrower than their overland counterparts and their modes are located at lower rain rates.

b. Azimuthal averages

The radial distributions of azimuthally averaged rain rates for each of the three storm intensity categories in the overland and overocean observations are shown in Fig. 2. The maximum azimuthal mean rain rate for all overland observations is about 1.6 mm h^{-1} within 50 km of the TC center (Fig. 1a), for all overocean observations it is about 5.0 mm h^{-1} (Fig. 1b), and for all mixed observations it is about 2.2 mm h^{-1} (Fig. 1c). For all overland, overocean, and mixed observations, the mean rain rate decreases to 1 mm h^{-1} at about 200, 250, and 300 km, respectively. For all overland, overocean, and mixed observations, rain rate decreases to 0.5 mm h^{-1} at about 400 km. Mean rain rates increase with storm intensity at all radii for all overland, overocean, and mixed observations. The peak mean rate and the location of the peak rainfall both vary with intensity for overland, overocean, and mixed groups (for detailed numbers, see Table 3).

Previous studies (Rodgers and Adler 1981; Rao and MacArthur 1994; Rodgers et al. 1994; Rodgers and Pierce 1995; Lonfat et al. 2004) on the radial distributions of azimuthally averaged rainfall rates of TCs showed characteristics similar to those seen in Fig. 2b for overocean observations, except that the values of rain-rate estimates had some differences because of using different kinds of observation means and different analysis resolutions or retrieval strategies, but the magnitude of these estimates showed no significant discrepancy. However, for overland distributions shown in Fig. 2a, significant differences from the overocean distribution can be identified, especially for the HUR category. It is obvious that correlations between rain rates and

TABLE 3. Peak rain rates and their locations from the storm center for each category as shown in Fig. 2.

	TD		TS		HUR	
	Peak rain rate (mm h^{-1})	Location (km)	Peak rain rate (mm h^{-1})	Location (km)	Peak rain rate (mm h^{-1})	Location (km)
Over ocean	1.8	70	2.5	70	8.0	40
Over land	1.0	70	2.2	70	9.5	15
Mixed	0.9	50	1.9	50	6.5	40

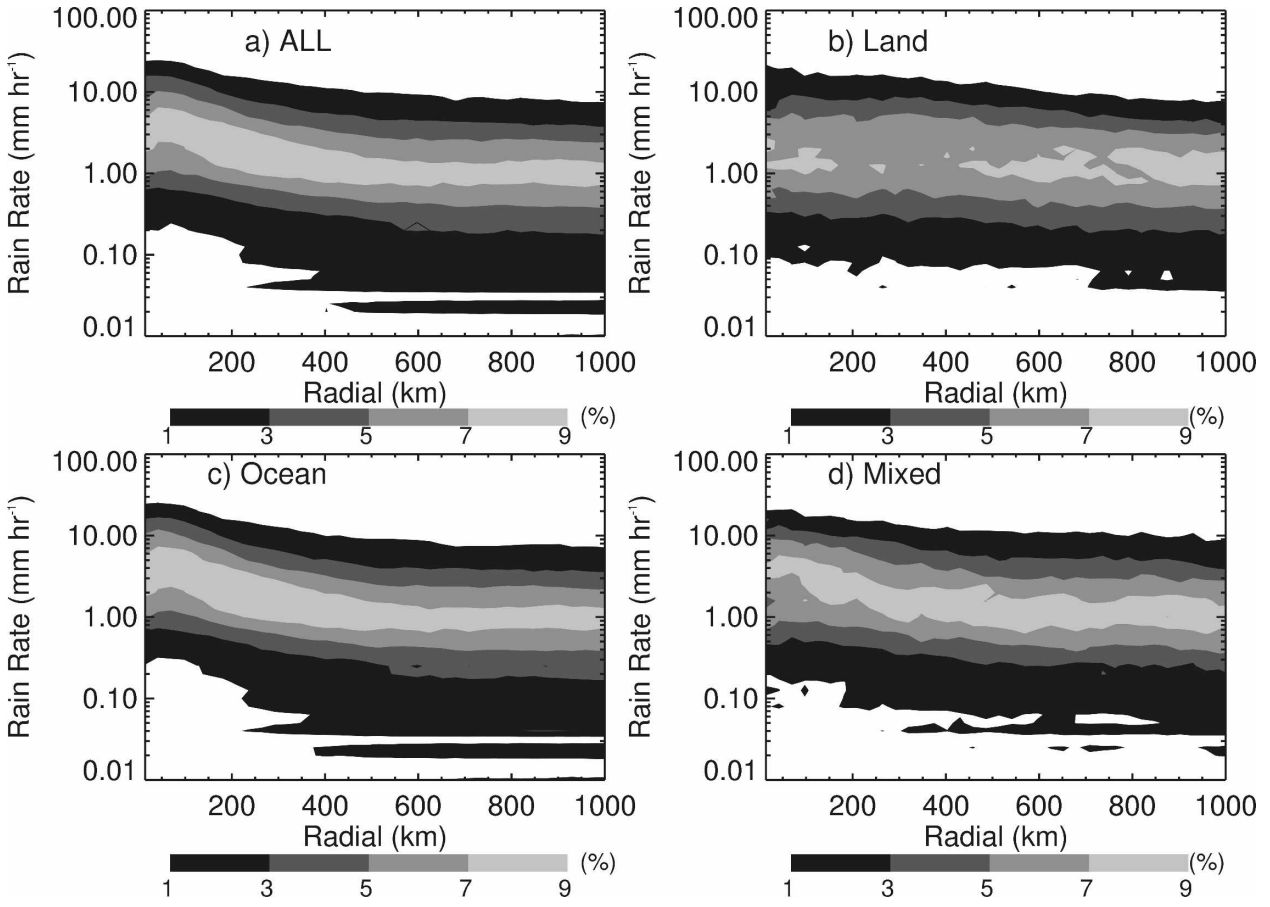

FIG. 3. Radial distribution of rainfall PDFs computed for (a) all 2680 observations, (b) overland observations, (c) overocean observations, and (d) mixed observations. The shading scale refers to the frequency of occurrence of rain rates at any radial distance from the storm center.

storm intensity still hold for overland observations but are weaker than those for overocean observations. For the HUR category, the peak rain rate for overland observations is higher and the location of this peak is much closer to the storm center than are those for overocean observations.

c. *Rain-rate distribution with radial distance*

Figures 3 and 4 show the rain-rate 2D frequency distributions with radial distance to the storm center. The 2D frequencies are computed outward to the 1111-km radius from the TC center. Figure 3 shows the 2D frequencies for all of the observations and for overland, overocean, and mixed observations. From Fig. 3a, the mode of the overall 2D frequency decreases from 4 mm h^{-1} in the inner 50 km to 1 mm h^{-1} by the 400-km radius. At ranges of more than 400 km, the peak remains at 1 mm h^{-1}. The overocean 2D frequency (Fig. 3c) is very similar to the overall distribution shown in Fig. 3a. Again, this is because the majority of the observations were over the ocean. The overland distribution shown in Fig. 3b is "flat"; the mode remains at about 1–1.5 mm h^{-1} for all radii. Overland observations have a broader distribution than do overall and overocean observations in the inner 200 km. The width of the distribution is a measure of the variability of TC rain (Lonfat et al. 2004). TCs over land seem to have a greater variability in the inner core. In the region beyond 200 km, the 2D frequency of overall and overocean TCs broadens, indicating an increase in the variability. The 2D frequency for mixed observations as shown in Fig. 3d indicates a translation of the rainfall distribution characteristics from over ocean to over land.

Figure 4 presents the 2D frequency distributions grouped by storm intensity for overland and overocean observations. The distributions vary with storm intensity. The mode of the land TD distribution (Fig. 4a) is around 1 mm h^{-1} for all radii, while the mode of the ocean TD distribution (Fig. 4b) decreases from

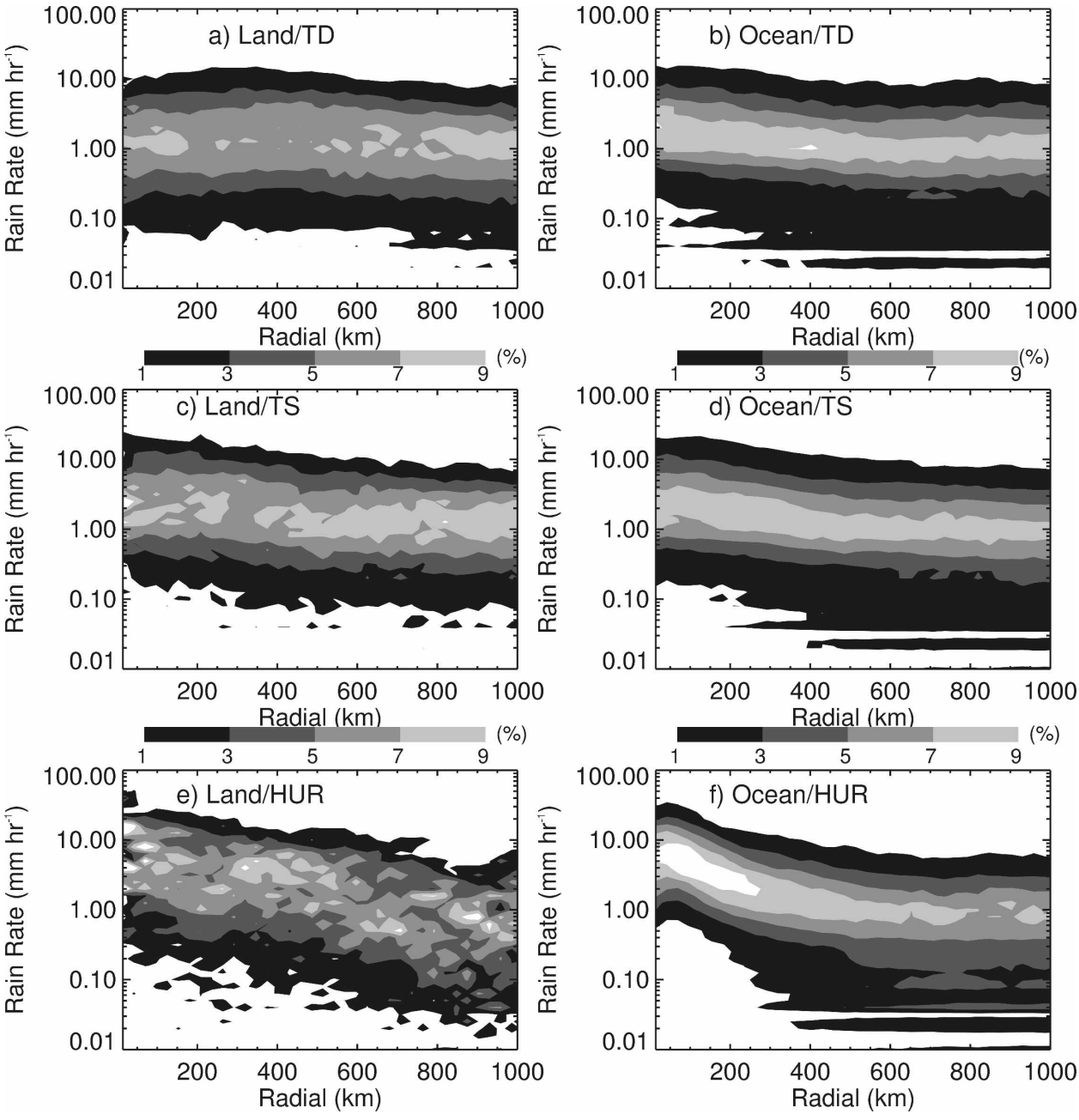

FIG. 4. Radial distribution of rainfall PDFs computed for (a) overland–TD, (b) overocean–TD, (c) overland–TS, (d) overocean–TS, (e) overland–HUR, and (f) overocean–HUR observations. The shading scale refers to the frequency of occurrence of rain rates at any radial distance from the storm center.

2 mm h^{-1} in the inner 100 km to 1 mm h^{-1} for the ranges of more than 100 km. The distribution of land TD is broader than that of ocean TD (note that the low rain rates in the ocean TD distribution in the region beyond 100 km are due to data noise). The mode of the land TS (ocean TS) distribution as shown in Fig. 4c (Fig. 4d) decreases from 2.5 (2.5) mm h^{-1} in the inner 100 km to 1.5 (0.9) mm h^{-1} for the ranges beyond 100 km. In general, the distribution of land HUR (Fig. 4e) is broader than that of ocean HUR (Fig. 4f) for all radii, indicating a greater variability of TC rainfall over land than over ocean. Multiple modes in the land HUR 2D frequency distribution are caused by noise resulting from the small sample size. However, the trend of rain rate decreasing with radius is still obvious, with the maximum rain rate of 10.5 mm h^{-1} in the inner 50 km,

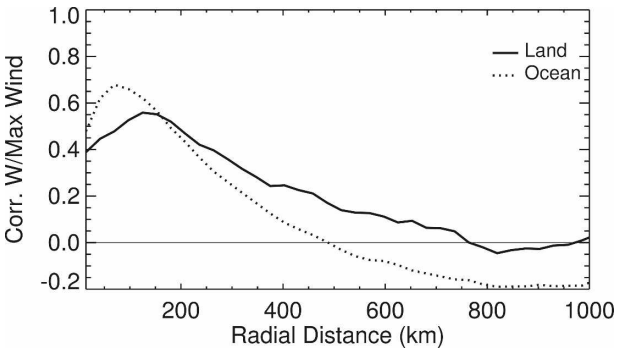

FIG. 5. Correlations between mean rain rate as a function of radial distance and TC maximum wind intensity for overland and overocean observations.

4 mm h^{-1} at 350-km radius, and around 0.5 mm h^{-1} at 1000-km radius. The mode of ocean HUR displays a smooth decrease from 7–8 mm h^{-1} in the inner 100 km to about 1 mm h^{-1} by the 400-km radius. The peak remains at 1 mm h^{-1} at ranges beyond 400 km.

d. Correlations with maximum wind intensity

Figure 5 demonstrates the correlations between mean rain rate as a function of radial distance and TC maximum wind intensity for overland and overocean observations. Table 4 lists these correlations for up to 3° radius. The highest correlation for the overocean observations is 0.68 at ~80-km radius. The highest correlation for the overland observations is 0.55 at ~120-km radius. It is obvious that, in the inner 150 km where the rain rate is highly correlated with the storm intensity, rain over land has a much weaker relationship with the storm maximum wind intensity than rain over ocean. From Fig. 5, we can also see that at ranges beyond 150 km from the TC center the correlations for overland rains are higher than those for overocean rain, but the values of correlations are generally so low that they will not be discussed. Meanwhile, significance tests show that correlations in Fig. 5 for radial distance of less than 400 km are statistically significant but that those for radial distance beyond 400 km are not.

Many studies (Rodgers et al. 1994, 2000; Rodgers and Pierce 1995) have shown that the inner-core (within 111-km radius) mean rain rate is a good indicator of storm intensity because the inner-core latent heat release that is directly related to the inner-core mean rain represents the major energy source for TC intensification. Figure 6 displays the storm maximum wind intensity as a function of inner-core mean rain rates for overland and overocean groups, respectively. In general, more intense TCs over land are associated with higher inner-core mean rain rate, but the overall correlation is

TABLE 4. Linear correlation coefficients between mean rain rate as a function of radial distance and TC maximum wind intensity for overland and overocean observations.

Radius (°)	0°–0.25°	0.25°–0.5°	0.5°–0.75°	0.75°–1°	1°–1.25°	1.25°–1.5°	1.5°–1.75°	1.75°–2°	1.75°–2°	2°–2.25°	2.25°–2.5°	2.5°–2.75°	2.75°–3°
Radial distance (km)	14	42	70	98	125	153	181	208	208	236	264	292	319
Coef for over land	0.39	0.45	0.48	0.53	0.56	0.55	0.52	0.47	0.47	0.42	0.40	0.36	0.32
Coef for over ocean	0.48	0.62	0.68	0.66	0.62	0.57	0.49	0.43	0.43	0.37	0.31	0.26	0.21

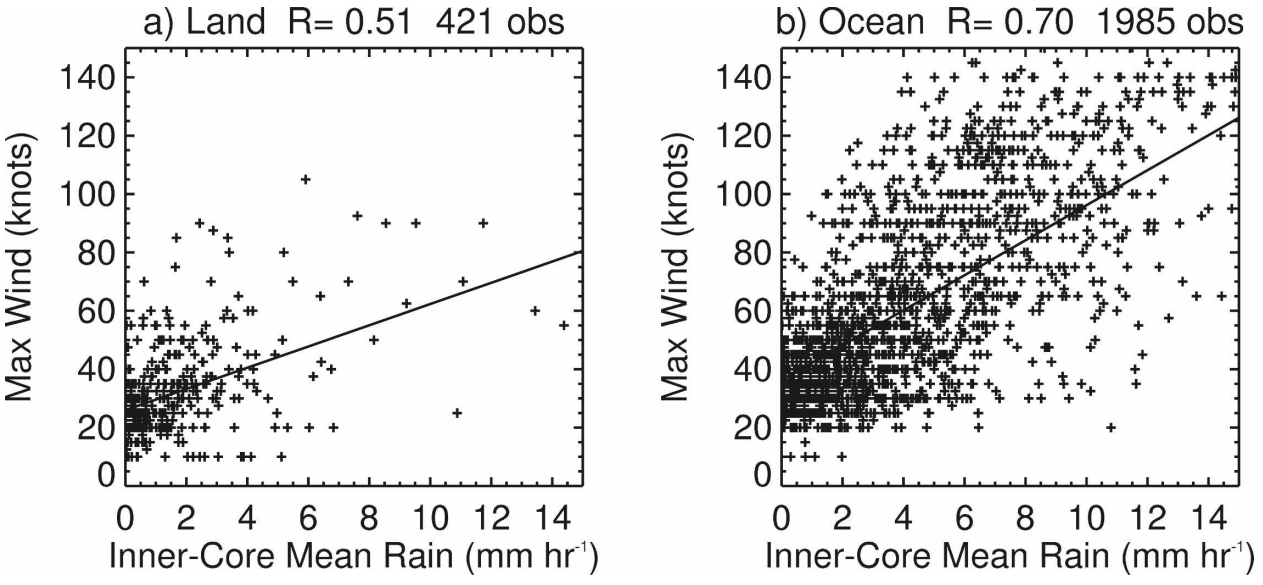

FIG. 6. Maximum wind intensity at the time of the MPA estimates as a function of inner-core (0°–1° radius) mean rain rate for (a) overland and (b) overocean observations.

only 0.51 and there is a large amount of scatter in the relationship (Fig. 6a). In the overocean scatterplot (Fig. 6b), although there are still many outliers, the correlation reaches 0.7, indicating that when TCs are over ocean the inner-core mean rain rate is correlated well with TC intensity. When TCs are over land, however, the correlation is much weaker.

4. Relationships between rain potential and TC landfall rain

One of the main questions in this study asks whether the rainfall potential when the storm is over the ocean could be used as a good predictor of the storm's expected rainfall over land. To test this, the relationships between a set of rainfall potential parameters for different time periods before landfall and the maximum storm total rain during the U.S. overland rain period are examined using the 1998–2004 Atlantic landfall TC dataset. A prediction index for TC overland rain is proposed and is verified by using an independent dataset including Atlantic landfall storms from 2005.

a. Relationships

The maximum storm total rain during the U.S. overland-rain period is obtained from surface rain gauge measurements. (See section 2b for a detailed definition of this parameter. For simplicity, in the following text, this parameter will be referred to as maximum storm total rain over land.) The rain gauge–based maximum storm total rain is our main parameter as the indicator of the TC rainfall over land. Rainfall potential derived from MPA data according to Eq. (1) is our predictor to be tested. Figure 7 shows the correlations between the maximum storm total rain over land and the rainfall

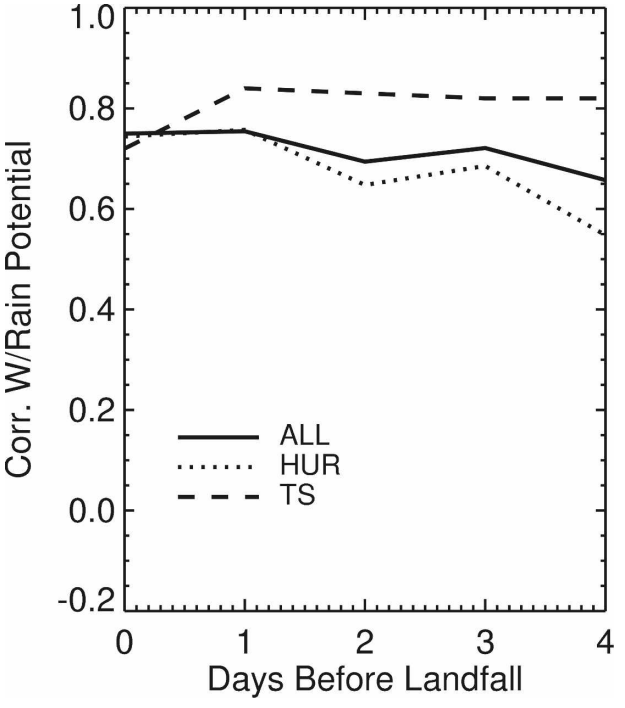

FIG. 7. Correlations between the maximum storm total rain over land and rainfall potential for 0–4 days before landfall for all tropical cyclones, HUR only, and TS only. HUR and TS represent the storm stage during landfall. The maximum storm total rain over land and rainfall potentials are in logarithmic scale.

TABLE 5. Linear correlation coefficients between the maximum storm total rain over land and rainfall potential for 0–4 days before landfall in the logarithmic scale for all samples (All), TCs with landfall intensity stage as hurricane (HUR), and TCs with landfall intensity stage as tropical storm (TS).

	All	HUR	TS
Rain potential on the landfall day	0.75	0.74	0.72
Rain potential for 1 day before landfall	0.75	0.76	0.84
Rain potential for 2 days before landfall	0.69	0.65	0.83
Rain potential for 3 days before landfall	0.72	0.69	0.82
Rain potential for 4 days before landfall	0.66	0.55	0.82

potential for 0–4 days before TC landfall for all 37 TCs that made landfall in the United States during 1998–2004 (see Table 1), subsamples that made landfall at hurricane stage (HUR; 13 storms), and those that made landfall at tropical storm stage (TS; 21 storms). These correlations are calculated in logarithm scale for both independent and dependent variables. Table 5 lists these correlations. Figure 7 clearly implies that the rainfall potential is highly correlated with the maximum storm total rain over land. It is apparent that the highest of these correlations (0.84) emerges from the TS sample with the rain potential for 1 day before landfall.

More insight into the relationships between TC overland rain and rainfall potential can be found by examining scatterplots of the data. Figure 8 presents scatterplots and linear correlations between the maximum storm total rain over land and rain potential for 1 day before landfall in logarithm scale for all tropical cyclones (Fig. 8a), landfall hurricanes (Fig. 8b), and landfall tropical storms (Fig. 8c). Only 36 storms are used in the linear correlation analysis in Fig. 8. Tropical Storm Allison (2001) is excluded because it made landfall on the first day of its lifetime and therefore no 1-day-before-landfall rainfall potential is available. However, a point on Fig. 8a for Allison (2001) is given by using the first day (landfall day) of rain of the storm to calculate the rainfall potential. From Fig. 8, in general, more intense TC overland rainfall is associated with high rainfall potential before TC's landfall. The correlations are 0.75, 0.76, and 0.84 for all samples, HUR samples, and TS samples, respectively. Significant tests for these correlations show that confidence levels are above 99%. However, there is a certain amount of scatter in the relationships. The greatest outlier is Hurricane Georges (1998). It is found that Georges made landfall in Key West, Florida, on 25 September 1998 and then went back to water. It made its second landfall in Biloxi, Mississippi, three days later. The maximum storm total rain over land actually occurred in Munson, Florida, which was related to the second landfall of Georges instead of its first landfall. After using the second landfall of Georges as the reference to calculate the rainfall potential, the agreement is much better (not shown here).

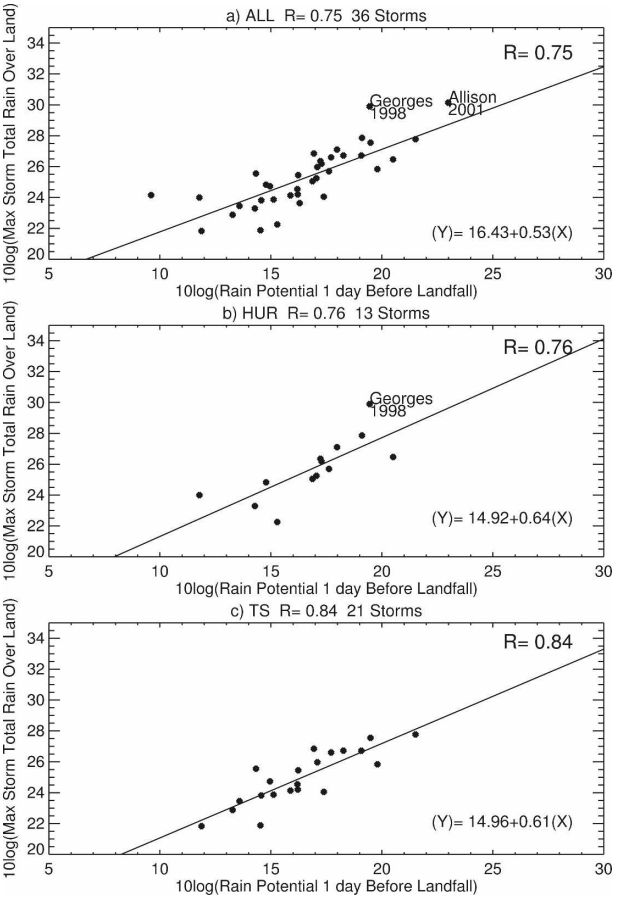

FIG. 8. Scatterplots and linear correlations between the maximum storm total rain over land (mm) and rain potential for 1 day before landfall in logarithmic scale (a) for all landfalling tropical cyclones, (b) for landfalling hurricanes, and (c) for landfalling tropical storms. The correlation coefficients and linear fit equations are also indicated. The rainfall potential of Allison (2001) is calculated by using the first day (landfall day) of rain of the storm. This storm is excluded from the linear correlation analysis.

b. *A prediction index for TC overland rain*

According to the logarithmically scaled linear fitting equation between the maximum storm total rain and rain potential for 1 day before landfall for all landfalling TCs (Fig. 8a), we have

$$\text{MaxRain} = 44(\text{RP})^{0.53}, \tag{2}$$

where MaxRain is the maximum storm total rain over land in millimeters and RP is the rain potential for 1 day before landfall, also in millimeters. This relationship is plotted in Fig. 9. A proposed prediction index for TC overland rain is given in Table 6 according to Fig. 9.

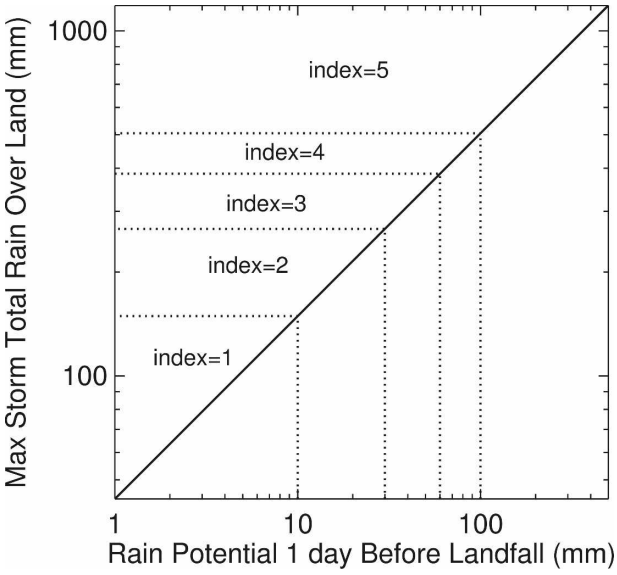

FIG. 9. Relationship between the maximum storm total rain over land and rainfall potential 1 day before landfall.

This index uses the rainfall potential for 1 day before landfall derived from the satellite-based MPA product to predict the maximum storm total rain over land. Five categories of TC landfall rain intensity are defined using this index. As the index increases from 1 to 5, the predicted TC maximum storm total rain over land increases from less than 149 mm (6 in.) to greater than 505 mm (20 in.). The index boundaries are chosen so that the breakpoint values for the maximum storm total rain over land (predicted parameter) are evenly spaced.

To verify this prediction index, independent cases that include six landfalling TCs over the Atlantic during the 2005 hurricane season are examined. These storms are Tropical Storm Arlene and Hurricanes Cindy, Dennis, Katrina, Rita, and Wilma. All of them made landfall in the U.S. Gulf Coast once except for Katrina, which made landfall twice: once over Florida on 26 August and once over Louisiana on 29 August 2005. Table 7 gives rainfall potentials derived from MPA for 1 day before landfall, predicted and observed maximum storm total rains over land, and the prediction errors for these six 2005 storms. By using Eq. (2), the average predicted maximum storm total rain over land of the seven landfalls is 367 mm; the corresponding observed value is 336 mm. The percentage error of this prediction is between 2.5% and 24.8%. Arlene, Katrina, and Rita are the storms whose landfall rain is predicted very accurately. However, the prediction for Cindy produces a 24.8% error, which is the highest among 2005 cases. The prediction for Wilma produces the second highest error, 18.1%. Also, the overland rain prediction indices for these two storms are predicted in the wrong category. We are able to exclude extratropical transition and topography interaction as the underlying reason. It is noticed, however, that the major assumption of this prediction technique is that the magnitude of rain rates does not change over the days before and after landfall. For the Hurricane Cindy case, the daily mean rain rate was 17.1 mm day^{-1} for 1 day before landfall and 9.8 mm day^{-1} on the landfall day, which represents a 43% decrease. This is the main reason for the overestimate of our prediction index for Cindy. For the Hurricane Wilma case, the storm accelerated at landfall, with a translation speed of 384 km day^{-1} on 1 day before landfall and 1067 km day^{-1} on the day of landfall. Because the translation speed is one of the three parameters in calculating the rainfall potential and because our daily averaging could not take this rapid speed change into account, an overestimate of Wilma's landfall rain is not surprising.

TABLE 6. TC overland rain prediction index.

Index	Rainfall potential for 1 day before landfall (mm)	Max storm total rain over land (mm)
1	<10	<149
2	10–30	149–267
3	30–60	267–385
4	60–100	385–505
5	≥100	≥505

5. Summary, discussion, and future work

Rainfall distributions over land and ocean for Atlantic TCs have been studied using observations from MPA. Between 1 January 1998 and 31 December 2004, 2680 three-hourly MPA measurements were collected in 37 Atlantic landfalling TCs with intensity ranging from a tropical depression to a category-5 hurricane. PDFs and azimuthal averages are constructed as a function of TC intensity and location. Correlations between rain rate and maximum wind intensity for overland and overocean observations are compared.

The PDF and azimuthal average analysis is used for comparison of MPA TC rainfall distributions with previous studies and to assess differences between overland and overocean samples. It is found that overocean distributions derived from the MPA product have characteristics that are similar to those results in previous studies (Rodgers et al. 1994; Rodgers and Pierce 1995; Lonfat et al. 2004). However, peak value and location of peak for overland distributions are significantly different from those for overocean distributions, indicating stronger rains for overland observations. Many previous studies (Rodgers et al. 1994, 2000; Rodgers and Pierce 1995) have shown that the inner-core mean rain

TABLE 7. Rainfall potentials derived from MPA for 1 day before landfall, predicted (Pred) and observed (Obs) maximum storm total rains over land, and the prediction errors for 2005 landfalling TCs over the North Atlantic basin.

2005 storms	Landfall date	Rainfall potential (mm)	Landfall rain prediction index		Max storm total rain over land (mm)		Error (%)
			Pred	Obs	Pred	Obs	
Arlene	11 Jun	29.3	2	2	264	250	5.6
Cindy	6 Jul	37.7	3	2	301	241	24.8
Dennis	10 Jul	55.0	3	3	368	325	13.2
Katrina	26 Aug	80.5	4	4	450	417	7.9
Katrina	29 Aug	55.4	3	3	367	376	2.5
Rita	24 Sep	70.3	4	4	419	406	3.2
Wilma	24 Oct	63.7	4	3	398	337	18.1
Avg					367	336	9.2

is correlated well with TC intensity. However, this study found that this statement might only be true for overocean observations. For TCs over land, the correlation is much weaker.

Using the same dataset, the relationships between rainfall potentials when the storm is over ocean and maximum storm total rain over land have been examined. A high correlation is found for the rainfall potential for 1 day before TC landfall. A prediction index is proposed based on this finding. Six landfalling TCs during the 2005 Atlantic hurricane season are analyzed to verify this prediction index. A comparison with surface rain gauge observations shows that the mean error of the forecast TC overland rain is 9.2%. According to this case study, the limitation of this technique is mainly associated with storms that show large changes in the rainfall magnitude and storm translation speed before and after landfall.

This study only uses factors related to the storm itself (rainfall history, storm size, and translation speed) to predict the TC overland rain. No environmental factors are considered. Two major environmental factors that are known to significantly enhance rain production during storm landfall are surface orography and extratropical transition. Many observational and modeling studies have examined the interactions of tropical cyclones with mountains (e.g., Geerts et al. 2000). Lonfat et al. (2007) developed a TC rainfall prediction model named the Parametric Hurricane Rainfall Model (PHRaM) that accounts for topography. The performance of PHRaM for 2004 U.S. landfalling storms showed significant improvement when compared with nontopography models when the storm interacted with terrains. During the extratropical transition (ET) of landfalling tropical cyclones over the United States, timing controls the interaction of poleward-moving tropical cyclones with westward-moving baroclinic disturbances, including upper-level troughs and jet streaks (Carr and Bosart 1978; Maddox et al. 1979). As the tropical cyclone remnants reintensify into a baroclinic extratropical cyclone, the precipitation distribution tends to broaden and to shift to the north and west of center (Elsberry 2002; Atallah 2002). Hurricane Agnes (1972) produced widespread severe flooding through the Northeast, with enhancement of the storm's high totals caused by orographic uplift along the Appalachian Mountains and coupled jet stream dynamics (DiMego and Bosart 1982).

To test whether the rainfall potential is still a good predictor for TC overland rain when ET happens, the 36 landfall TCs used in Fig. 8 are grouped by ET storms and non-ET storms according to the NHC best-track information. Figure 10 presents scatterplots and linear correlations between the maximum storm total rain over land and rain potential for 1 day before landfall in

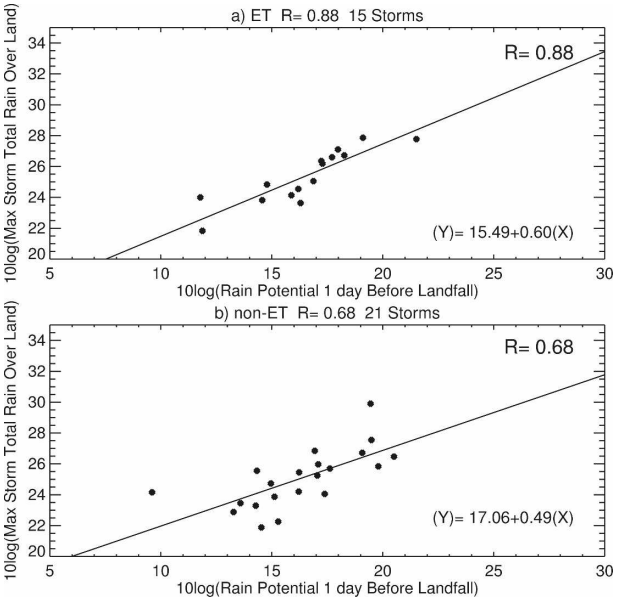

FIG. 10. Scatterplots and linear correlations between the maximum storm total rain over land (mm) and rain potential for 1 day before landfall in logarithmic scale for (a) ET and (b) non-ET storms. The correlation coefficients and linear fit equations are also indicated.

logarithmic scale for ET and non-ET storms. Surprising is that the ET group produces a higher correlation (0.88) than the non-ET group (0.68). This result demonstrates that the rainfall potential–based TC overland rain prediction index is robust enough to predict the peak rainfall regardless of the ET condition. This may reflect the fact that the peak rainfall in ET and non-ET cases is similar for similar overocean conditions in the storm. However, in relation to flooding, another key issue is where the rainfall occurs, and understanding ET is critical in that respect. Next, we plan to conduct individual case studies to estimate the actual effect of ET on TC inland flooding on both rainfall maximum and on rainfall locations. Terrain interactions will also be part of future work.

Acknowledgments. The authors thank Drs. Robert Adler and George Huffman for providing MPA data. Thanks are given to Drs. David Roth and James Franklin for their assistance on TC surface rainfall and best-track data. Thanks are given, too, for discussion and feedback from Drs. Frank Marks and Scott Braun. The constructive suggestions from Dr. Manuel Lonfat and another anonymous reviewer resulted in substantial improvements to the manuscript. This research was supported by the NASA Precipitation Measurement Missions (PMM) Grant NNX07AL41G. The authors thank Ramesh Kakar (NASA Headquarters) for his continued support of PMM science.

REFERENCES

Adler, R. F., A. J. Negri, P. R. Keehn, and I. M. Hakkarinen, 1993: Estimation of monthly rainfall over Japan and surrounding waters from a combination of low-orbit microwave and geosynchronous IR data. *J. Appl. Meteor.,* **32,** 335–356.

——, G. J. Huffman, and P. R. Keehn, 1994: Global tropical rain estimates from microwave-adjusted geosynchronous IR data. *Remote Sens. Rev.,* **11,** 125–152.

——, and Coauthors, 2003: The version 2 Global Precipitation Climatology Project (GPCP) monthly precipitation analysis (1979–present). *J. Hydrometeor.,* **4,** 1147–1167.

Atallah, E. H., 2002: An evaluation of precipitation distribution in landfalling tropical cyclones. Preprints, *25th Conf. on Hurricanes and Tropical Meteorology,* San Diego, CA, Amer. Meteor. Soc., 339–340.

——, and L. F. Bosart, 2003: The extratropical transition and precipitation distribution of Hurricane Floyd (1999). *Mon. Wea. Rev.,* **131,** 1063–1081.

Carr, F. H., and L. F. Bosart, 1978: A diagnostic evaluation of rainfall predictability for tropical storm Agnes, June 1972. *Mon. Wea. Rev.,* **106,** 363–374.

Demuth, J. L., M. DeMaria, and J. A. Knaff, 2006: Improvement of Advanced Microwave Sounding Unit tropical cyclone intensity and size estimation algorithms. *J. Appl. Meteor. Climatol.,* **45,** 1573–1581.

DiMego, G. J., and L. F. Bosart, 1982: The transformation of Tropical Storm Agnes into an extratropical cyclone. Part II: Moisture, vorticity, and kinetic energy budgets. *Mon. Wea. Rev.,* **110,** 412–433.

Elsberry, R. L., 2002: Predicting hurricane landfall precipitation. *Bull. Amer. Meteor. Soc.,* **83,** 1333–1340.

——, 2005: Achievement of USWRP hurricane landfall research goal. *Bull. Amer. Meteor. Soc.,* **86,** 643–645.

Ferraro, R., and Coauthors, 2005: The tropical rainfall potential (TRaP) technique. Part II: Validation. *Wea. Forecasting,* **20,** 465–475.

Geerts, B., G. M. Heymsfield, L. Tian, J. B. Halverson, A. Guillory, and M. I. Mejia, 2000: Hurricane Georges's landfall in the Dominican Republic: Detailed airborne Doppler radar imagery. *Bull. Amer. Meteor. Soc.,* **81,** 999–1018.

Griffith, C. G., W. L. Woodley, P. G. Gube, D. W. Martin, J. Stout, and D. N. Sikdar, 1978: Rain estimates from geosynchronous satellite imagery: Visible and infrared studies. *Mon. Wea. Rev.,* **106,** 1153–1171.

Heymsfield, G. M., J. B. Halverson, J. Simpson, L. Tian, and T. P. Bui, 2001: ER-2 Doppler radar investigations of the eyewall of Hurricane Bonnie during the Convection and Moisture Experiment-3. *J. Appl. Meteor.,* **40,** 1310–1330.

Huffman, G. J., R. F. Adler, M. M. Morrissey, D. T. Bolvin, S. Curtis, R. Joyce, B. McGavock, and J. Susskind, 2001: Global precipitation at one-degree daily resolution from multisatellite observations. *J. Hydrometeor.,* **2,** 36–50.

——, and Coauthors, 2007: The TRMM Multisatellite Precipitation Analysis (TMPA): Quasi-global, multiyear, combined-sensor precipitation estimates at fine scales. *J. Hydrometeor.,* **8,** 38–55.

Jiang, H., J. B. Halverson, and J. Simpson, 2008a: On the difference of storm rainfall of Hurricanes Isidore and Lili. Part I: Satellite observations and rain potential. *Wea. Forecasting,* **23,** 29–43.

——, ——, ——, and E. J. Zipser, 2008b: On the difference of storm rainfall of Hurricanes Isidore and Lili. Part II: Water budget. *Wea. Forecasting,* **23,** 44–61.

Kidder, S. Q., M. D. Goldberg, R. M. Zehr, M. DeMaria, J. F. W. Purdom, C. S. Velden, N. C. Grody, and S. J. Kusselson, 2000: Satellite analysis of tropical cyclones using the Advanced Microwave Sounding Unit (AMSU). *Bull. Amer. Meteor. Soc.,* **81,** 1241–1259.

——, J. A. Knaff, S. J. Kusselson, M. Turk, R. R. Ferraro, and R. J. Kuligowski, 2005: The tropical rainfall potential (TRaP) technique. Part I: Description and examples. *Wea. Forecasting,* **20,** 456–464.

Kummerow, C., W. S. Olson, and L. Giglio, 1996: A simplified scheme for obtaining precipitation and vertical hydrometeor profiles from passive microwave sensors. *IEEE Trans. Geosci. Remote Sens.,* **34,** 1213–1232.

Lonfat, M., F. D. Marks, and S. S. Chen, 2004: Precipitation distribution in tropical cyclones using the Tropical Rainfall Measuring Mission (TRMM) Microwave Imager: A global perspective. *Mon. Wea. Rev.,* **132,** 1645–1660.

——, R. Rogers, T. Marchok, and F. D. Marks Jr., 2007: A parametric model for predicting hurricane rainfall. *Mon. Wea. Rev.,* **135,** 3086–3097.

Maddox, R. A., C. F. Chappell, and L. R. Hoxit, 1979: Synoptic and mesoscale aspects of flash flood events. *Bull. Amer. Meteor. Soc.,* **60,** 115–123.

Malkus, J., and H. Riehl, 1960: On the dynamics and energy transformations in steady-state hurricanes. *Tellus,* **12,** 1–20.

Miller, B. I., 1958: Rainfall rates in Florida hurricanes. *Mon. Wea. Rev.,* **86,** 258–264.

Rao, G. V., and P. D. MacArthur, 1994: The SSM/I estimated rainfall amounts of tropical cyclones and their potential in predicting the cyclone intensity changes. *Mon. Wea. Rev.,* **122,** 1568–1574.

Rappaport, E. N., 2000: Loss of life in the United States associated with recent Atlantic tropical cyclones. *Bull. Amer. Meteor. Soc.,* **81,** 2065–2074.

Rodgers, E. B., and R. F. Adler, 1981: Tropical cyclone rainfall characteristics as determined from a satellite passive microwave radiometer. *Mon. Wea. Rev.,* **109,** 506–521.

——, and H. F. Pierce, 1995: A satellite observational study of precipitation characteristics in western North Pacific tropical cyclones. *J. Appl. Meteor.,* **34,** 2587–2599.

——, S. W. Chang, and H. F. Pierce, 1994: A satellite observational and numerical study of precipitation characteristics in western North Atlantic tropical cyclones. *J. Appl. Meteor.,* **33,** 129–139.

——, W. Olson, J. Halverson, J. Simpson, and H. F. Pierce, 2000: Environmental forcing of Supertyphoon Paka's (1997) latent heat structure. *J. Appl. Meteor.,* **39,** 1983–2006.

Rogers, R., S. Chen, J. Tenerelli, and H. Willoughby, 2003: A numerical study of the impact of vertical shear on the distribution of rainfall in Hurricane Bonnie (1998). *Mon. Wea. Rev.,* **131,** 1577–1599.

Weng, F., L. Zhao, R. Ferraro, G. Poe, X. Li, and N. Grody, 2003: Advanced Microwave Sounding Unit cloud and precipitation algorithms. *Radio Sci.,* **38,** 8068–8079.

Zhao, L., and F. Weng, 2002: Retrieval of ice cloud parameters using the Advanced Microwave Sounding Unit. *J. Appl. Meteor.,* **41,** 384–395.